ADVANCES IN ATMOSPHERIC SCIENCES, VOL. 33, JULY 2016, 852–864

Spatiotemporal Variability of Methane over the Amazon from Satellite Observations

Igor Oliveira RIBEIRO[1], Rodrigo Augusto Ferreira de SOUZA[*2], Rita Valéria ANDREOLI[2], Mary Toshie KAYANO[3], and Patrícia dos Santos COSTA[1]

[1]*Post-Graduate Program in Climate and Environment, CLIAMB, INPA/UEA, Av. André Araújo,* 2936, *Campus II, Aleixo,* 69060-001, *Manaus, AM, Brasil*

[2]*Amazonas State University, Superior School of Technology, Av. Darcy Vargas,* 1200, *Parque 10 de Novembro,* 69065-020, *Manaus, AM, Brasil*

[3]*National Institute for Space Research, Center For Weather Forecasting and Climate Research, Av. dos Astronautas,* 1758, 12227-010, *São José dos Campos, SP, Brasil*

(Received 10 June 2015; revised 14 January 2016; accepted 23 January 2016)

ABSTRACT

The spatiotemporal variability of the greenhouse gas methane (CH_4) in the atmosphere over the Amazon is studied using data from the space-borne measurements of the Atmospheric Infrared Sounder on board NASA's AQUA satellite for the period 2003–12. The results show a pronounced variability of this gas over the Amazon Basin lowlands region, where wetland areas occur. CH_4 has a well-defined seasonal behavior, with a progressive increase of its concentration during the dry season, followed by a decrease during the wet season. Concerning this variability, the present study indicates the important role of ENSO in modulating the variability of CH_4 emissions over the northern Amazon, where this association seems to be mostly linked to changes in flooded areas in response to ENSO-related precipitation changes. In this region, a CH_4 decrease (increase) is due to the El Niño-related (La Niña-related) dryness (wetness). On the other hand, an increase (decrease) in the biomass burning over the southeastern Amazon during very dry (wet) years explains the increase (decrease) in CH_4 emissions in this region. The present analysis identifies the two main areas of the Amazon, its northern and southeastern sectors, with remarkable interannual variations of CH_4. This result might be useful for future monitoring of the variations in the concentration of CH_4, the second-most important greenhouse gas, in this area.

Key words: climate variability, methane, satellite data, Amazon region

Citation: Ribeiro, I. O., R. A. F. de Souza, R. V. Andreoli, M. T. Kayano, and P. S. Costa, 2016: Spatiotemporal variability of methane over the Amazon from satellite observations. *Adv. Atmos. Sci.*, **33**(7), 852–864, doi: 10.1007/s00376-016-5138-7.

1. Introduction

Methane (CH_4) is the most abundant hydrocarbon in the atmosphere and one of the main greenhouse gases, responsible for 20% of the warming due to the long-lived greenhouse gases. After the end of the pre-industrial era, its concentration first rose globally, then stabilized from 1999 to 2006, and has since been increasing again (Dlugokencky et al., 1998; UNFCCC, 2008; Bousquet et al., 2011). Previous studies have shown low CH_4 concentration rates during the 1990s and 2000s, except in the periods 1997–98 and 2002–03 when peaks in CH_4 emissions occurred (Ciais et al., 2013; WMO, 2013). Several explanations for this low CH_4 concentration have been proposed: (1) a decrease in global emissions related to fossil fuels (Levin et al., 2012); (2) compensation of the increase in anthropogenic emissions by reduced emissions from wetlands (Bousquet et al., 2006; Dlugokencky et al., 2009; Bousquet et al., 2011; Pison et al., 2013); and (3) a decrease in emissions due to anthropogenic activities, in particular in the countries of the former Soviet Union (Simpson et al., 2012). According to a report from the Ministry of Science, Technology and Innovation of Brazil, published in 2013, on annual estimates of greenhouse gas emissions in Brazil (MCTI, 2013), the emissions of these gases over the Amazonian biomass were reduced from 2004 onwards due to the changes in environmental and resource policies for the regulation of land and forest use.

According to the WMO (2013), the concentration of CH_4 in 2012 was approximately 1819 parts per billion by volume (ppb), which indicated an increase of 260% compared with the pre-industrial year of 1750. The variation in the CH_4 concentration is an important aspect of climate change, because this gas is part of the atmospheric chemistry of ozone and hy-

* Corresponding author: Rodrigo SOUZA
Email: souzaraf@gmail.com

droxyl radicals, and is approximately 25 times more effective than carbon dioxide in absorbing longwave radiation (IPCC, 2013; Cressot et al., 2014; Tate, 2015). The increase in the CH_4 concentration originates from natural and anthropogenic (e.g., fossil fuel combustion) sources, mainly over wetlands. Globally, total emissions are two-thirds due to anthropogenic processes and one-third due to natural processes, albeit with uncertainties in terms of the individual contribution of each source (Kirschke et al., 2013; Cressot et al., 2014). The seasonal variations of CH_4 emissions in the tropics, particularly over Brazil, are modulated by biomass burning, mainly during the dry season, and by wetlands during the wet season, where flooded areas favor a high rate of primary emissions and decomposition (Chen and Prinn, 2006; Simpson et al., 2006; van der Werf et al., 2006; Bousquet et al., 2011; Kirschke et al., 2013). Natural emissions from wetlands are the largest single source of CH_4, and most of these emissions originate from the tropics.

During ENSO events, planetary-scale changes in ocean temperature occur in the tropics, producing anomalies in soil temperature and precipitation. As a result, ENSO could play a significant role in determining the interannual variability of wetland emissions. Hodson et al. (2011) quantified the influence of interannual variability associated with ENSO on wetland CH_4 emissions, and showed that global wetland CH_4 variability is strongly related to ENSO variability. The results also showed that the variability in tropical wetland CH_4 emissions is due mainly to the variations in flooded areas. So, variations in precipitation associated with ENSO can explain the variability of tropical CH_4.

Although the main sources and sinks of CH_4 are known, quantification of its emissions contains uncertainties, because ground-based measurements are quite sparse in several regions of the globe (Walter et al., 2001a). Furthermore, data obtained from aircraft also have low spatial and temporal resolutions due to limitations in measurement procedures. However, as one of the few trace gases with a spectral signature, CH_4 can be observed from a space-borne sounder. The Atmospheric Infrared Sounder (AIRS) on board the NASA/AQUA satellite was the first advanced atmospheric infrared sounder of high spectral resolution. It was tailored to provide information on several greenhouse gases and to study the water and energy cycles (Le Marshall et al., 2006). Several studies have used the measurements from AIRS to describe spatial and temporal variabilities in the emissions and transportation of atmospheric gases (Park et al., 2004; Xiong et al., 2009a; Zhang et al., 2011; Rajab et al., 2012). AIRS measurements have been used to show the variability of the CH_4 concentration and its increase over different regions (Xiong et al., 2010; Zhang et al., 2011; Rajab et al., 2012). The estimated CH_4 values have been validated with aircraft and surface measurements (Xiong et al., 2008, 2010: Zhang et al., 2011). A comparison between *in–situ* measurements and AIRS-CH_4 over China at different tropospheric levels (200, 300 and 400 hPa) made by Zhang et al. (2011) showed they have similar seasonal cycles. Nevertheless, Xiong et al. (2009b) showed that AIRS-CH_4 over South Asia is significantly affected by the vertical transport of CH_4 from the boundary layer to the middle troposphere. Similarly, the strong convective activity over the Amazon may make it possible to link AIRS-CH_4 with surface emissions. Based on ground-based observational and remote sensing satellite data, Zhang et al. (2013) analyzed the precision of different CH_4 concentrations remotely sensed by NASA/AQUA, GOSAT (Greenhouse Gases Observation Satellite) and SCanning Imaging Absorption spectroMeter for Atmospheric CHartographY (SCIAMACHY) and the results showed that the tropospheric CH_4 concentration data from AIRS provided better results of surface observations over time, as well as its seasonal trends. These results support the use of the AIRS products to examine the CH_4 seasonal cycle and its variability.

The present analysis examines the spatiotemporal variability of the CH_4 in the atmosphere over the Amazon region using 10 years of data obtained by the NASA/AQUA satellite. The following section describes the data and methodology. Section 3 discusses the climatological and anomalous features of CH_4 and the possible causes of these features. Conclusions are drawn in section 4.

2. Data and methodology

The eight-day means of the mixing rate of CH_4 at three pressure levels (200, 300 and 400 hPa) obtained from the NASA/AQUA satellite, V5, were used. These data are available at a $1^\circ \times 1^\circ$ resolution (http://mirador. gsfc.nasa.gov/) for the period 2003–12. The SVD method was used for CH_4 retrieval based on the 7.66-μm band with high spectral resolution (Susskind et al., 2003; Xiong et al., 2008, 2009a). Validation by *in-situ* aircraft observations from 2003 to 2007 showed that the bias of the retrieved CH_4 profiles is approximately −1.4% to 0.1%, and its RMSE is around 0.5%–1.6% (Xiong et al., 2008, 2010). The uncertainties include errors in atmospheric temperature and water moisture profiles, surface temperature and emissivity over high-altitude land, the noise of sensors, and errors in cloud clearing (Xiong et al., 2009a). However, some of these errors are more pronounced in the Asian monsoon region, where the contrast between high and low monsoon phases is reflected in relatively rapid variations of the atmospheric temperature, water moisture and convection. In fact, Xiong et al. (2008) argued that the increase in moisture imported by the Asian monsoon to the Tibetan Plateau region pushes the most sensitive region of AIRS CH_4 channels to higher altitudes, which also leads to some moisture-dependent artifacts in the seasonal variation of the retrieved CH_4. The largest difference in monthly averaged AIRS CH_4 between September and May 2004 at upper tropospheric layers occurs over the Tibetan Plateau. In contrast, this difference for the 450–550 hPa layer is approximately 40 ppb over the Amazon (Xiong et al., 2008, Fig. 9). Considering that this layer is close to the level used here, and this difference of approximately 2% of the monthly value in May and September is larger than the uncertainty of 0.5%–1.6% in the AIRS retrieval, the existence of artifacts in the seasonal variations of the AIRS retrieval is irrelevant

for the purposes of the present analysis. The TRMM-based three-hourly precipitation estimates, V7, available at http://disc.sci.gsfc.nasa.gov/precipitation/, were also used. For details on the algorithm used to estimate the TRMM precipitation, see Huffman et al. (2007). These data are gridded at a 0.25° ×0.25° resolution and were obtained in the area limited to (5.5°N–12.5°S, 47.5°–75.5°W), the Amazon region, for the period 2003–12 period. Eight-day-averaged TRMM precipitation data were calculated.

In order to examine the seasonal cycle of the CH_4 and precipitation over the Amazon, boxplots of these time series were produced. Five quantities are shown in a boxplot: the lower (25%) and upper (75%) quartiles are the lower and upper borders of the box; the median (the horizontal segment inside the box); and the minimum and maximum values (vertical lines extending from the box) (Wilks, 2006). The boxplot also depicts the outliers. The monthly CH_4 and precipitation boxplots provide information on their seasonal characteristics and are useful for exploratory analyses of these variables. The relationships between the seasonal cycles of the CH_4 and precipitation time series averaged over the Amazon were examined through linear correlation.

The anomaly time series of CH_4 and precipitation were obtained for each grid point over the Amazon by considering the means of the period 2003–12. The linear trend for this period in the time series was removed at each grid point. The dominant variability mode of CH_4 was obtained by subjecting the anomaly time series of this variable to EOF analysis. The EOF calculations were based on the correlation matrix. To assess the statistical significance of a correlation coefficient different from zero, the number of degrees of freedom was estimated as the recorded length divided by the time interval of two independent realizations, which is the lag needed to obtain autocorrelation coefficients of the principal component (PC) time series close to zero. The number of degrees of freedom was 45. Using a two-tailed Student's *t*-test, it was found that correlations above 0.3 are significantly different from zero correlation at the 95% level of confidence. So, only correlation values above 0.3 were considered in our analysis.

The detrended precipitation anomaly time series averaged over the Amazon was also obtained. The time-frequency variations of the PC of the first and second EOF mode and the detrended precipitation anomaly time series over the Amazon were obtained through wavelet analyses. The relationships between the variations of CH_4 concentration and the precipitation anomaly time series were examined by calculating the wavelet coherence and phase differences between PC01 and the precipitation anomaly time series.

The time-frequency analysis was performed using the Morlet wavelet, a complex exponential wave modulated by a Gaussian function, $e^{i\omega_o\eta}e^{-\eta^2/2}$, with $\eta = t/s$, where t is the time, s is the wavelet scale, and ω_0 is a non-dimensional frequency. Following Torrence and Compo (1998), the wavelet function at each scale s is normalized by $s^{-1/2}$. This normalization allows comparisons of the wavelet transform among scales s and among the transform of other time series. The Global Wavelet Power (GWP) for a given scale s is the time average over all the local wavelet power spectra, and is given by equation 22 in Torrence and Compo (1998) as:

$$\overline{W}^2(s) = \frac{1}{N}\sum_{n=0}^{N-1}|W_n(s)|^2 \ .$$

$W_n(s)$ is the wavelet transform of a discrete sequence, n is the time index and s is the scale. Given two time series, $X(t)$ and $Y(t)$, with wavelet transforms $W_X(t,s)$ and $W_Y(t,s)$, the cross-wavelet spectrum is defined as $W_{XY}(t,s) = W_X(t,s)W_{Y*}(t,s)$, where $(*)$ is the complex conjugate. The squared wavelet coherence is defined as the squared modulus of the smoothed cross-wavelet spectrum, normalized by smoothed wavelet spectra (Torrence and Webster, 1999):

$$R^2(t,s) = \frac{|\langle s^{-1}W_{XY}(t,s)\rangle|^2}{\langle s^{-1}W_X(t,s)\rangle\langle s^{-1}W_Y(t,s)\rangle} \ ,$$

where $< >$ denotes smoothing in both time and scale. The factor s^{-1} converts the squared wavelet coherency into an energy density. The wavelet coherency phase difference is given by

$$\Delta\Phi(t,s) = \tan^{-1}\frac{\Im m\{\langle s^{-1}W_{XY}(t,s)\rangle\}}{\Re e\{\langle s^{-1}W_{XY}(t,s)\rangle\}} \ ,$$

where $\Im m$ and $\Re e$ are the imaginary and real parts of $W_{XY}(t,s)$, respectively (Torrence and Webster, 1999).

3. Results and discussion

3.1. *Seasonal features of CH_4 and precipitation over the Amazon*

Figure 1 shows the time series of CH_4 at pressure levels of 200, 300 and 400 hPa, and that of precipitation. The CH_4 concentration shows a decrease with altitude, and the most sensitive layer of AIRS-CH_4 to be used for analysis is at 400 hPa. This is consistent with CH_4 vertical profiles over the Amazon obtained from an aircraft for the period 2010–13, whose higher CH_4 concentration occurred for levels closer to the surface than for higher levels (Basso, 2014). This happens because flooded areas, water reservoirs and lakes act as CH_4 sources. With altitude, the CH_4 concentration lowers due to various factors such as wind transport, losses into the stratosphere, and chemical reactions with hydroxyl radicals. For all levels, CH_4 shows similar seasonal variations, with the greatest values occurring during the dry season (August to November) and the smallest during the wet season (February to May). The same seasonal variations of CH_4 in the Amazon region have been previously noted (Walter et al., 2001b; Costa et al., 2011). Also, the lowest CH_4 concentration values in the study period occur from 2004 to 2008, and the highest during 2003 and from 2009 onwards. Furthermore, an increase in CH_4 is noted at the beginning of 2008. According to Dlugokencky et al. (2009), this increase is more likely

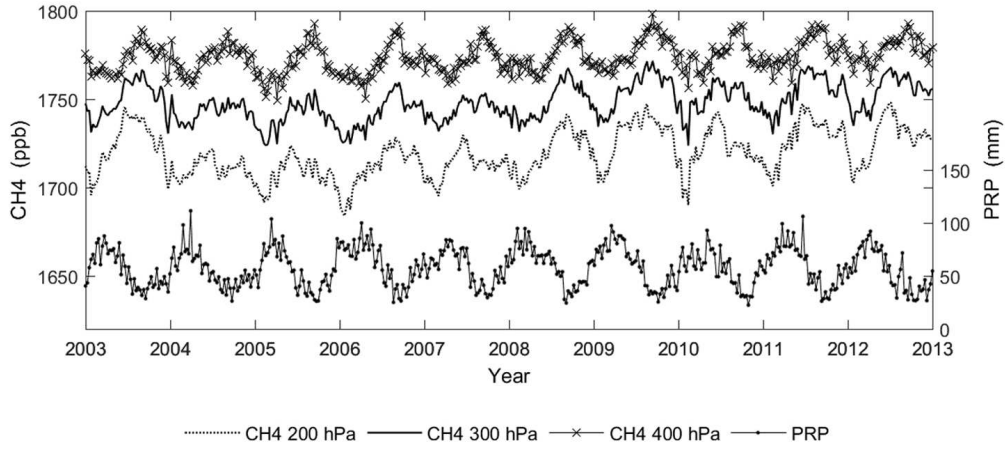

Fig. 1. Time series of the eight-day mean CH_4 concentration at 200 hPa, 300 hPa and 400 hPa, and the eight-day mean precipitation, averaged over the Amazon.

related to positive precipitation anomalies in the tropics than to biomass burning. They also found that this increase in CH_4 in the tropics was responsible for the increase in the global average value (by 4.4 ± 0.6 ppb) in that year.

Zhang et al. (2011) found that the CH_4 from AIRS and from in-situ measurements present very similar seasonal cycles over China. Considering that this behavior of CH_4 might occur over the Amazon, and that the CH_4 at the three analyzed levels shows very similar seasonal cycles (Fig. 1), the subsequent analyses are for the CH_4 at the 400-hPa level only.

The boxplots of the precipitation and 400-hPa CH_4 time series are shown in Figs. 2 and 3, respectively. Both time series show a well-defined seasonal cycle, with the peak in the precipitation leading that in the CH_4 concentration by five to six months. A consistent seasonal cycle of the CH_4 concentration was previously found for smaller areas over the Amazon (Costa et al., 2011). This time lag between the two peaks corresponds to the time interval necessary for the enlargement of flooded areas, a favorable condition for a large amount of biomass decomposition, which in turn causes substantial CH_4 emissions into the atmosphere during the subsequent dry season.

The highest precipitation values from February to May, with the highest median in March, define the wet season; and the lowest values from August to September, with the lowest median in September, define the dry season (Fig. 2). The time interval of six months between the highest and lowest medians indicates a symmetrical seasonal cycle. The highest level of dispersion occurs in June during the transition period from wet to dry season, and the lowest in October within the dry season. Outliers above the upper quartile in most months, except for June and December, indicate a high frequency of extreme rainfall events. On the other hand, outliers below the first quartile occur in March and April. This indicates outbreaks of rain during the wet season.

The CH_4 boxplot shows the highest CH_4 concentration values from July to October, with the highest median in September; while the lowest values occur in the February–May period, with the lowest median in April (Fig. 3). The time interval of seven months between the highest and lowest medians, and that of five months between the lowest and highest medians, indicate an asymmetric seasonal cycle. In general, the period with the highest CH_4 concentrations overlaps that with the lowest precipitation values. Two main factors contribute to the occurrence of higher CH_4 concentrations during the dry season: the climatological decrease of flooded areas in the flat lands of the Amazon, and the biomass burning in the arc of the deforestation region, which favors land use, and takes part in a cyclical process modulated by the climatological rainfall distribution. The highest level of dispersion occurs in April, during the period with the lowest CH_4 concentrations. This highest level of dispersion might be related to the precipitation, because April is also the month with precipitation outliers on both sides of the box, which are above the upper quartile and below the lower quartile. The lowest level of dispersion occurs in September, in the period with the highest CH_4 concentrations. The outlier above the upper quartile in September is likely due to the biomass burning during the dry season.

The linear correlation of -0.68 between these two time series indicates that nearly 46% of the CH_4 seasonal cycle variance is explained by the precipitation seasonal variability. This region has a pronounced dry season and a rainy season modulated by the meridional displacement of the ITCZ (Fisch et al., 1998). Consequently, the Amazon river level shows an annual fluctuation of approximately 10 m (Junk, 1970; Richey et al., 1986), which is accompanied by flooding of the large lowland areas or wetlands, favoring high primary emission rates and decomposition (Chen and Prinn, 2006; Simpson et al., 2006; van der Werf et al., 2006; Bousquet et al., 2011; Kirschke et al., 2013). Consistent with these results, Walter et al. (2001b) and Ringeval et al. (2010) found that the seasonal cycle of CH_4 emissions in the tropical wetlands is modulated by the rainfall seasonal cycle. The higher CH_4 fluxes from the Amazonian rivers during the low-water season may be explained by the greater dilution of incoming CH_4 from sediments and groundwater, and the greater time for CH_4 oxidation in deeper water columns during high-

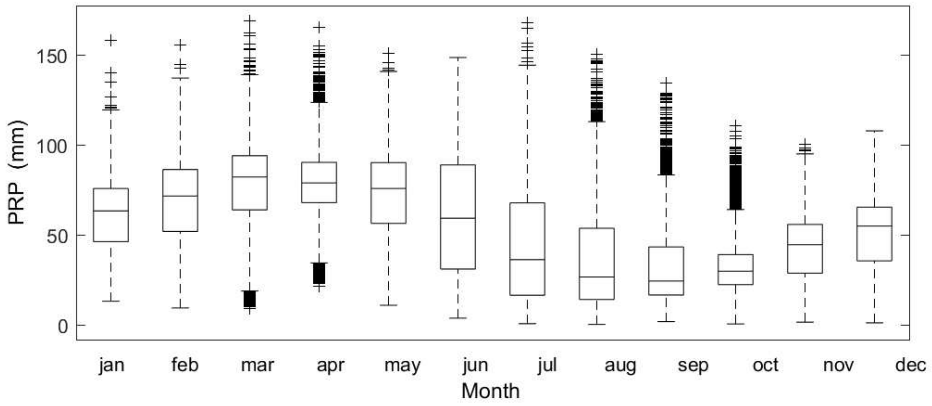

Fig. 2. Monthly boxplot of the eight-day mean precipitation (PRP) over the Amazon basin for the period 2003–12.

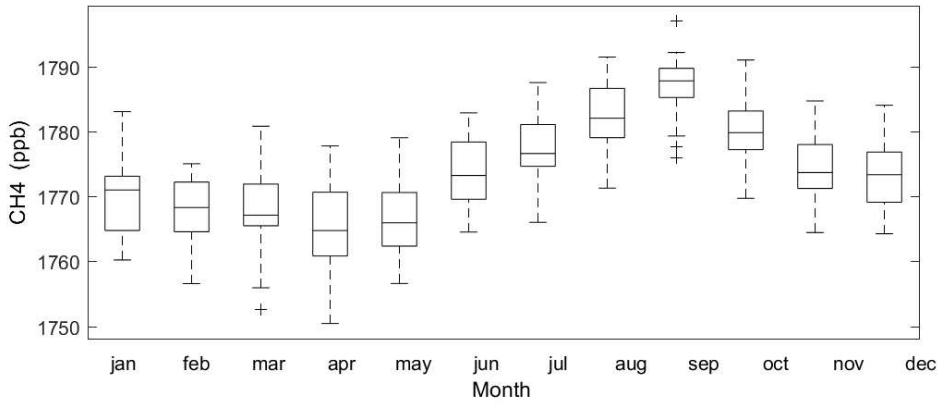

Fig. 3. Monthly boxplot of the eight-day mean 400-hPa CH_4 over the Amazon basin for the period 2003–12.

water periods (Sawakuchi et al., 2014). Both effects could contribute to the lower values observed during the high-water season.

3.2. *Dominant 400-hPa CH_4 variability*

The dominant variability mode of the 400-hPa CH_4 concentration over the Amazon basin and its temporal variations are depicted in Fig. 4. This mode shows the largest positive anomalies over the northern sector of the Amazon Basin, mainly along the Amazon River, which contains over 350 000 km^2 of wetlands (Melack and Hess, 2011). The high and low regimes of this river alter the wetlands, and consequently more deeply influence CH_4 emissions into the atmosphere. The corresponding PC01 shows low-frequency variations superimposed on interannual variations, and explains 20.8% of the total variance (Fig. 4). The 400-hPa CH_4 anomaly time series averaged over the Amazon (figure not shown) exhibits variations similar to those illustrated in the PC01 time series. Thus, a large part of the 400-hPa CH_4 variations over the Amazon can be attributed to its northern portion.

The second variability mode of CH_4 (Fig. 5) shows the largest anomalies centered in the southeastern sector of the basin, in the deforestation arc region. In this region, the CH_4 variability is related to biomass burning, in particular during the dry season. The corresponding PC02 shows seasonal and interannual variations, and explains 8% of the total variance.

The PC01 time series features low-frequency variations with dominance of negative values during the 2004–08 period, and positive ones from mid-2008 onwards, which are superimposed on interannual variations (Fig. 4). For the interannual timescale, the negative PC01 values during the first half of 2005, 2007 and 2010 coincide with the El Niño events of 2004–05, 2006–07 and 2009–10, respectively; and the positive PC01 values during the second half of 2005, during 2008–09, during the first half of 2011, and during 2012, coincide with the La Niña events of 2005–06, 2007–08, 2008–09 and 2011–12, respectively. The El Niño and La Niña years can be found at www.cpc.ncep.nooa.gov. For the negative (positive) PC01 values, negative (positive) CH_4 anomalies prevail over the northern sector of the Amazon Basin. Consistent with the study of Hodson et al. (2011), the results here also indicate a clear relationship between the CH_4 interannual variations and ENSO, such that the CH_4 emissions from the wetlands of the northern Amazon reduce (increase) in response to El Niño-related (La Niña-related) dry (wet) conditions in that region. Furthermore, these results are consis-

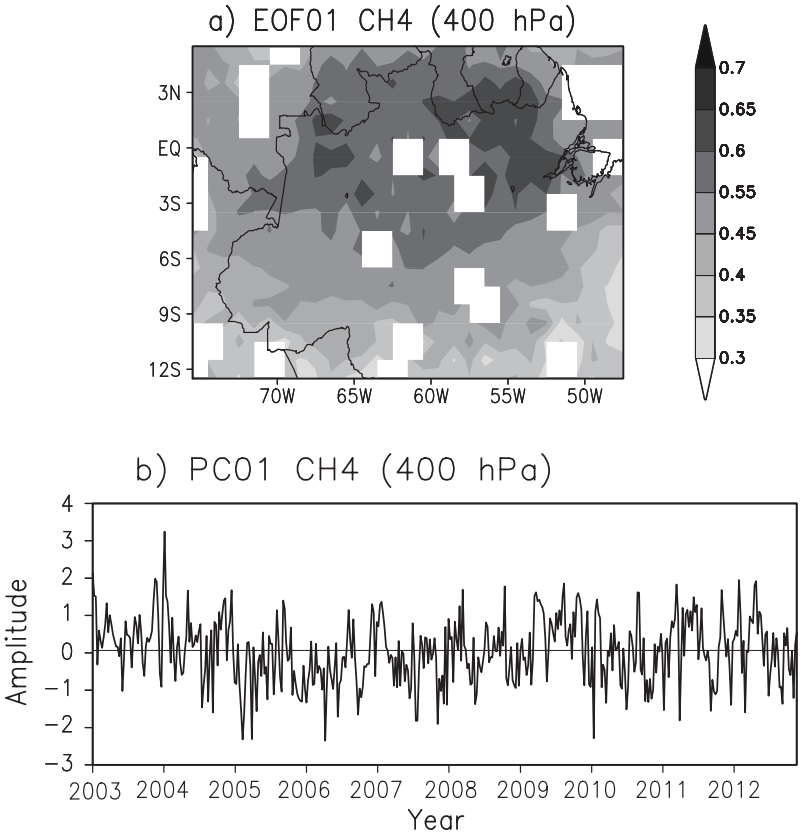

Fig. 4. First EOF mode pattern of the 400-hPa CH_4 monthly anomalies (a), and the corresponding PC time series (b). The interval in (a) is 0.05, and the grey-shaded areas with correlation values above 0.3 are significantly different from zero correlation at the 95% level of confidence. The gaps are areas where there are no data.

tent with the previously documented global decrease in CH_4 emissions over the 1999–2007 period (Bousquet et al., 2006; Dlugokencky et al., 2009; Bousquet et al., 2011; Pison et al., 2013), and the increase in the CH_4 concentration in the atmosphere during 2007 and 2008, attributed to the above-normal precipitation in the tropics (Bousquet et al., 2011).

On the other hand, the high positive (negative) PC02 values during 2006, 2007 and 2008 (the end of 2009 and the end of 2010) indicate an increased (reduced) CH_4 concentration (Fig. 5). The positive peaks of PC02 are associated with biomass burning over the southeastern Amazon. In this case, the increase in the carbon monoxide emissions due to biomass burning contributes to the increase in CH_4 concentration, mainly in the southeastern sector of the study domain (Worden et al., 2013). Under very dry conditions, associated with El Niño, as in 2010 (Lewis et al., 2011), the biomass burning might have contributed to the CH_4 increase in the region.

The results here show that 28.8% of the CH_4 total variance over the Amazon is due to the precipitation variability, being 20.8% (first mode) related to variations in the flooding in the northern sector of the study domain, which occur in response to the precipitation variability, and 8% (second mode) related to the biomass burning in the southeastern sector of the region. The present study indicates a stronger influence of ENSO on the variation in CH_4 emissions from flooded areas than from the biomass burning during the last decade. This result confirms previous findings obtained on a global basis (Hodson et al., 2011),

The time-frequency variations of the PC01 time series obtained from the wavelet analysis are illustrated in Fig. 6. The GWP of this time series shows a significant 4–8-yr interannual peak (maximum at 7 yr), and secondary non-significant peaks at 2.5 yr and 0.7 yr (Fig. 6c). The strong 4–8-yr interannual GWP values are due to the significant interannual variances during almost the whole period of analysis (Fig. 6b). The 2.5-yr GWP peak is due to the high variances at the 2–4-yr timescale during the whole period of analysis, with significant values from mid-2008 to mid-2010. The 0.7-yr GWP peak is due to the significant variances at this timescale during the period from mid-2004 to mid-2005, and in 2011. This analysis indicates that the PC01 contains the dominant variability at the 4–8-yr timescale. In other words, the CH_4 over the northern sector of the Amazon basin, and mostly along the Amazon River, shows a dominant 4–8-yr variability.

The time-frequency variations of the PC02 time series obtained from the wavelet analysis are illustrated in Fig. 7. The GWP of this time series shows a significant 0.5–1-yr peak and a secondary non-significant peak at 2.5 yr (Fig. 7c). The

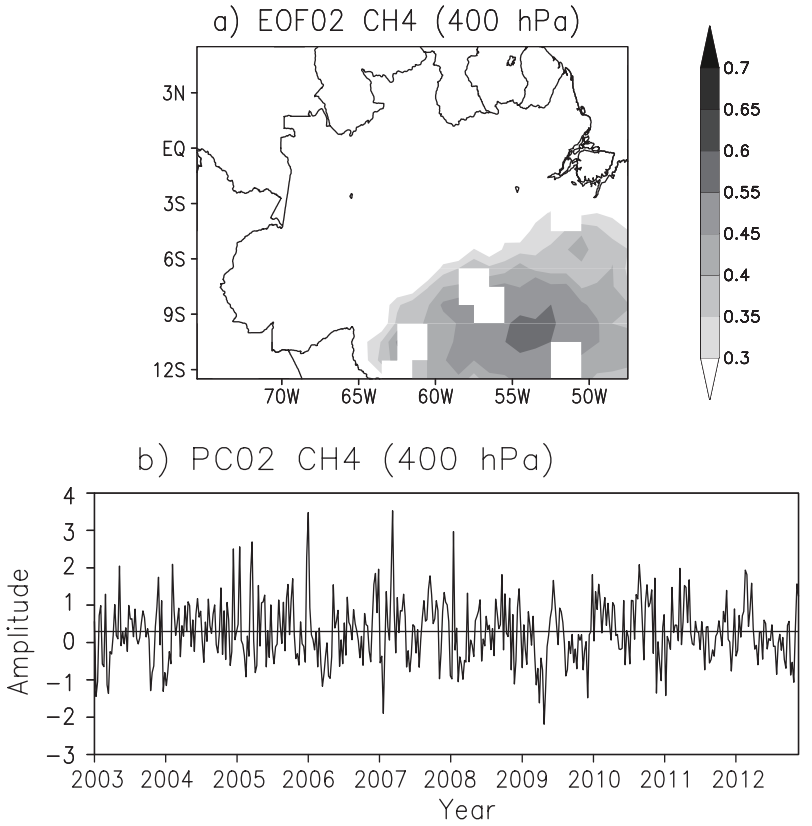

Fig. 5. As in Fig. 4 but for the second EOF mode pattern of the 400-hPa CH_4 monthly anomalies and the corresponding PC time series.

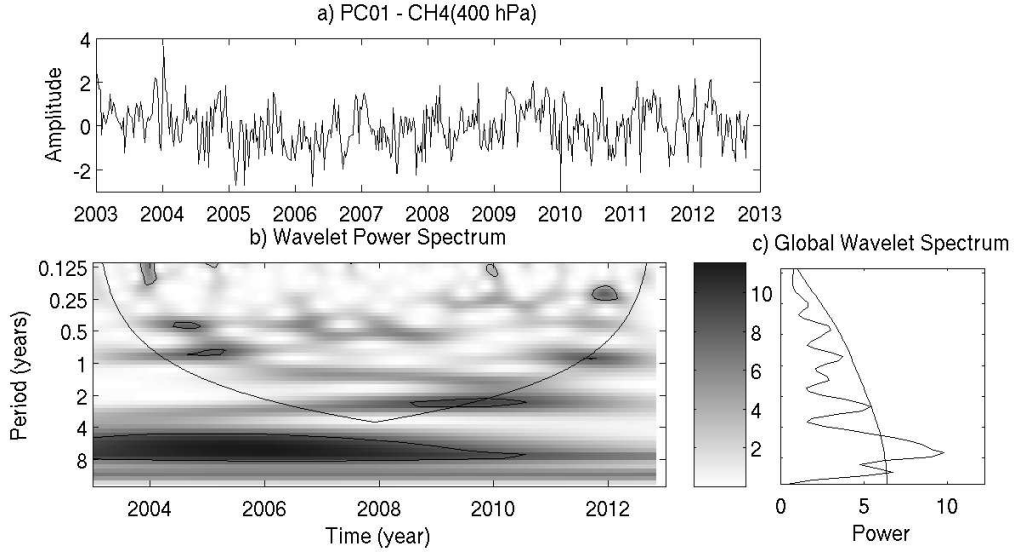

Fig. 6. The (a) PC01 time series and (b) local wavelet power spectrum of the continuous wavelet transform of PC01, normalized by $1/\sigma^2$ ($\sigma^2 = 1$). (c) Global Wavelet Power (in variance units). The closed contours in (b) encompass significant variances at the 95% confidence level, and the region where the edge effects are important is under the U-shaped curve in (b). The convex curve in (c) is the significance at the 5% level, assuming a red-noise spectrum.

strong 0.5–1-yr GWP values are due to the significant semi-annual variances from 2009 to 2011 (Fig. 7b). The 2.5-yr GWP peak is due to the variances at the 2–4-yr timescale during the whole period of analysis, with non-significant values. This analysis indicates that the PC02 contains the dominant variability at the 0.5–1-yr and 2–4-yr timescales. In other

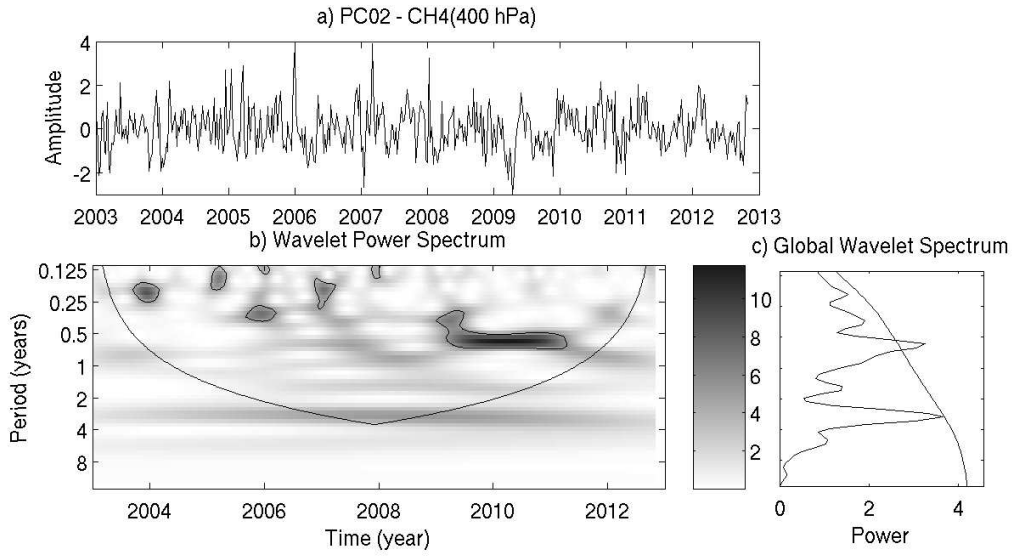

Fig. 7. As in Fig. 6 but for PC02.

words, CH_4 over the southeastern sector of the Amazon basin shows two dominant scales of variability, the annual and interannual.

Since precipitation has a significant impact on CH_4 emissions in the tropics, it is expected that emissions also vary during an ENSO event due to the variations in rainfall (Hodson et al., 2011). So, the interannual PC01 and PC02 variability might also be related to the precipitation variability associated with ENSO. Thus, the relationships between the PC01, PC02 and precipitation anomaly time series are examined. First, the time-frequency variations of the precipitation anomaly time series are analyzed (Fig. 8). The GWP of this time series features a significant 2–4-yr interannual peak (maximum at 2.5 yr), and secondary non-significant peaks at 0.5, 1 and 1.5 yr (Fig. 8c). The strong significant interannual GWP values are due to the significant interannual variances during the period from 2007 to the end of 2011 (Fig. 8b). A GWP peak at 11 yr is also apparent. However, in this case the variances do not show significant values. The period with high 2–4-yr interannual variances for the precipitation anomaly time series overlaps the period with significant variance for this timescale for the PC01 and PC02 time series. Thus, at least for this timescale, the PC01 and PC02 variations are likely related to the precipitation variability.

The relationships between the PC01, PC02 and precipitation anomaly time series are examined from the cross-wavelet analysis for these two time series (Figs. 9 and 10). The precipitation anomaly time series and the PC01 show significant coherence at the 0.5–1-yr timescale from 2003 to mid-2006, with phase differences of 180°, and at the 0.25–0.5-yr timescale from mid-2007 to mid-2010, with phase differences of −90° (Fig. 9). For the 0.5–1-yr timescale, the phase difference of 180° indicates that a maximum in precipitation coincides with a minimum in CH_4 emissions. For the 0.25–0.5-yr timescale, the phase difference of −90° indicates that the maximum in precipitation leads the maximum in CH_4 emissions by 20 to 45 days. These time series also show significant coherence at the 2–4-yr timescale from 2004 onwards, because both time series contain high 2–4-yr interannual variability during the common period from 2005 to 2011. In this case, the phase differences between the precipitation and PC01 time series vary from −45° to −90°. For a 2-yr (4-yr) timescale, the maximum in the precipitation leads the maximum in the PC01 by 3–6 (6–12) months. This lead/lag association between the precipitation and PC01 can be interpreted in terms of the ENSO-related interannual rainfall variations over the Amazon. The La Niña-related (El Niño-related) wet (dry) conditions over the Amazon contribute to an enhancement (a reduction) of flooded areas, meaning the CH_4 emissions from these areas increase (reduce). For the 2–4-yr timescale, the results here indicate that the increase (decrease) in CH_4 emissions lags the maximum positive (negative) La Niña-related (El Niño-related) precipitation anomalies by 3–12 months.

The precipitation anomaly time series and the PC02 show significant coherence at the 0.25–0.5-yr timescale during the end of 2005, beginning of 2006, beginning of 2008, and beginning of 2010, with the phase difference varying from −45° to +45° (Fig. 10). Significant coherence at the 0.5–1-yr timescale occurs during 2007 and 2008, and at the 1–2-yr scale during 2005 and 2006, with a phase difference of +90°. In this case, considering the 1-yr timescale, a phase difference of +90° indicates that a minimum in the precipitation occurs about six months before the maximum in CH_4 emissions. Significant coherence at the 1.5–4-yr timescale occurs during 2007, 2008 and 2009, with the phase differences varying from 90° to 145°. In this case, considering the timescale with the largest levels of coherence, for the 2-yr timescale, a phase difference of 90° (145°) means that a minimum or a maximum in the precipitation time series occurs about 9 (15) months before the minimum or the maximum in the CH_4 time series. This lead/lag association between the precipitation

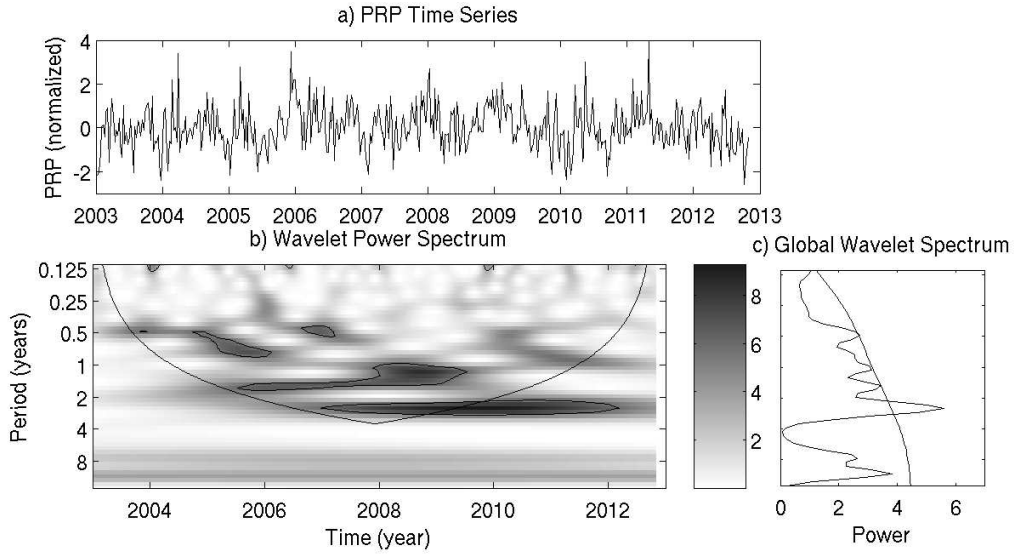

Fig. 8. The (a) precipitation (PRP) anomaly time series and (b) local wavelet power spectrum of the continuous wavelet transform of the precipitation, normalized by $1/\sigma^2$ ($\sigma^2 = 118.8$ mm^2). (c) Global Wavelet Power (in variance units The closed contours in (b) encompass significant variances at the 95% confidence level, and the region where the edge effects are important is under the U-shaped curve in (b). The convex curve in (c) is the significance at the 5% level, assuming a red-noise spectrum.

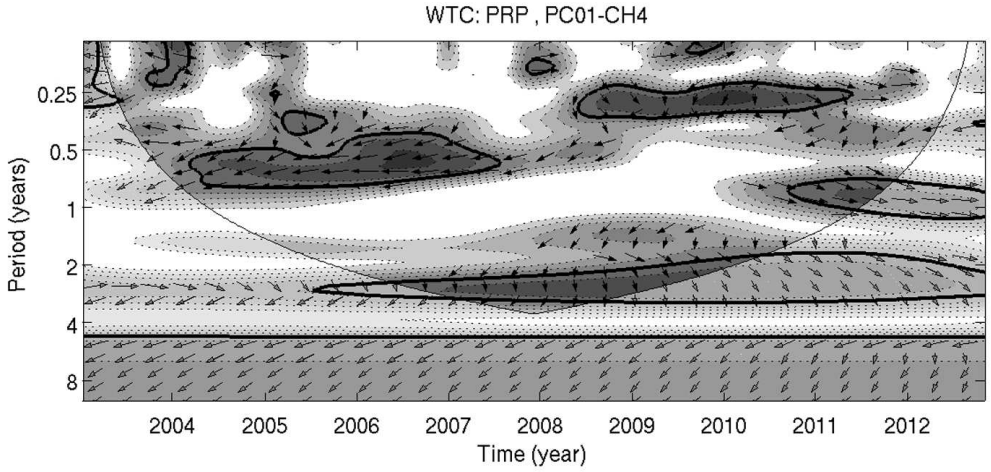

Fig. 9. Squared wavelet coherence and phase differences between the precipitation anomaly time series and the PC01 illustrated in Fig. 4. Dotted contours and shading represent wavelet squared coherence and vary from 0.3 to 1.0, with intervals of 0.1. The region where the edge effects are important is under the U-shaped curve. Arrows indicate the phase differences as follows: in-phase (0°), pointed to the right; antiphase (180°), pointed to the left; the first time series leading the second one by 90°, pointed downward; and the first time series lagging the second one by 90°, pointed upward.

and PC02 can be interpreted in terms of the ENSO-related interannual rainfall variations over the southeastern Amazon. The La Niña-related (El Niño-related) wet (dry) conditions over this region contribute to reduce (intensify) the biomass burning, so that CH_4 emissions due to this activity are reduced (enhanced). For a 2-yr timescale, our results indicate that the decrease (increase) in CH_4 emissions due to the reduced (intensified) biomass burning lags the La Nina-related (El Niño-related) wetness (dryness) by 9–15 months.

3.3. *Relationships between CH_4 tendency and ENSO*

In order to confirm the relationships between the variation in CH_4 and ENSO, the CH_4 time series tendency, defined as the CH_4 difference between two subsequent years, is compared with the seasonal Oceanic Niño Index (ONI) obtained at http://www.cpc.ncep.noaa.gov/products/analysis_monitoring/ensostuff/ensoyears.shtml. A positive (negative) CH_4 tendency indicates an increase (a decrease) in the CH_4 concentration. In order to obtain a smooth time se-

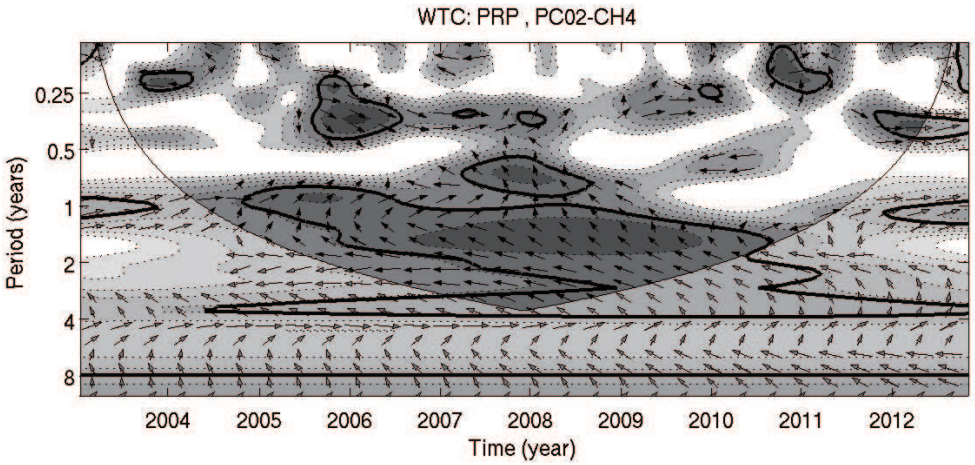

Fig. 10. As in Fig. 9 but for the squared wavelet coherence and phase differences between the precipitation anomaly time series and the PC02 illustrated in Fig. 5.

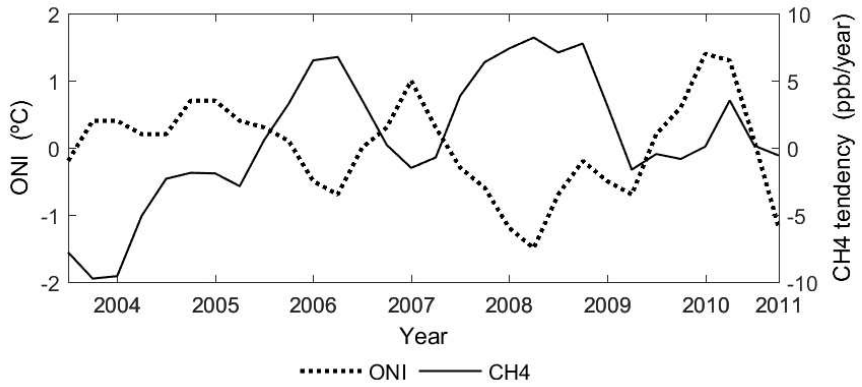

Fig. 11. Seasonal 400-hPa CH_4 tendency and the Oceanic Niño Index (ONI) time series for April–May–June 2003 to October–November–December 2010.

ries, nine-month-averaged CH_4 values are obtained and attributed to the central month. These average CH_4 values are obtained for February, May, August and November. Subsequently, four CH_4 tendency values are obtained for each year. The ONI values for the trimesters of January–February–March, April–May–June, July–August–September and October–November–December are then compared with the CH_4 tendency time series. These time series are obtained for the period from August 2003 to November 2010 (Fig. 11). This figure clearly illustrates a negative correlation between the CH_4 tendency and the ONI time series. So, under La Niña years, indicated by the negative ONI values, the CH_4 concentration increases due to the enlarged flooded areas caused by above-normal rainfall over the region. Indeed, the positive CH_4 tendency values from mid-2005 to mid-2006 and from mid-2007 to the end of 2008 coincide with the occurrence of moderate and strong La Niña events during these periods. On the other hand, during the El Niño years (2006–07 and 2009–10), the negative CH_4 tendency values indicate a slightly reduced CH_4 emission rate, due to the dry conditions related to this event. Therefore, the differences seem to be due to the changes in flooded areas, which are in turn associated with variations in the precipitation. Remember that under El Niño-related dryness, such as in 2010 (Lewis et al., 2011), the biomass burning might have contributed to increased CH_4 over the southeastern Amazon, as discussed above for PC02. The intensification of burning due to El Niño-related dryness increases CH_4 emissions into the atmosphere (Worden et al., 2013) and compensates the expected decrease in CH_4 emissions due to the shrinking of flooded areas. These results confirm the aforementioned relationship between ENSO and the dominant CH_4 variability mode reported in subsection 3.3.

4. Conclusions

The eight-day mean atmospheric CH_4 concentration data obtained from sounding sensors on board the NASA/AQUA satellite allow detailed analyses of the spatiotemporal variations of this variable over the Amazon region. Consistent with previous works, in general, the highest concentrations occur at 400 hPa, rather than at higher levels, because this level is closer to the emission sources of this gas, such as

flooded areas, water reservoirs, lakes and others. In the higher levels, the CH_4 concentration decreases due to several factors, such as wind transport, losses into the stratosphere, and chemical reactions with the hydroxyl radicals in the atmosphere. However, the CH_4 at the three analyzed levels shows similar seasonal cycles. The CH_4 concentration in all analyzed levels shows a well-defined seasonality, with a maximum during the dry season (August to November) and a minimum during the wet season (February to May). The seasonal precipitation and 400-hPa CH_4 time series show well-defined seasonal cycles, with a peak in the precipitation leading that in the CH_4 concentration by five to six months. This result is consistent with previous findings for smaller areas over the Amazon (Costa et al., 2011). This time lag between the two peaks corresponds to the time interval necessary for the enlargement of flooded areas—a favorable condition for a large amount of biomass decomposition, which causes substantial CH_4 emissions into the atmosphere during the dry season.

Our results indicate a clear relationship between CH_4 interannual variations and ENSO, such that the emissions of CH_4 from the wetlands of the northern Amazon are reduced (increased) due to the El Niño-related (La Niña-related) dry (wet) conditions in that region. Consistent results are obtained from the analysis of the relationships between the CH_4 tendency, defined on an annual basis, and the ONI. In this analysis, the increase in the CH_4 concentration from mid-2005 to mid-2006, and from mid-2007 to the end of 2008, might be justified by the emissions from flooded areas, due to the above-normal rainfall associated with the La Niña events of 2005–06 and 2007–08. Also, the decrease in the CH_4 concentration noted from the end of 2006 to the beginning of 2007, and in 2009, is related to the dry conditions in the region associated with El Niño events. These results are consistent with the previously documented global decrease in CH_4 emissions over the period 1999–2007 (Bousquet et al., 2006; Dlugokencky et al., 2009; Bousquet et al., 2011; Pison et al., 2013), and the increase in the atmospheric CH_4 concentration during 2007 and 2008, attributed to the above-normal precipitation in the tropics (Bousquet et al., 2011).

On the other hand, the CH_4 variability over the southeastern Amazon is associated with the variability in biomass burning. Under very dry conditions, such as during 2007–10 (Lewis et al., 2011), biomass burning can easily get out of control, due to the excessively dry vegetation, leading to high CH_4 emissions. During El Niño events, the intensification of burning is related to increases in CH_4 emissions (Worden et al., 2013). According to data made available at the Burning and Fire Monitoring website of the National Institute for Space Research (http://www.dpi.inpe.br/proarco/bdqueimadas), the southeastern Amazon experienced a high burning index during the second semester of 2010. This caused an increase in CH_4 emissions in this region during 2010. Furthermore, the biomass burning during 2010 might have compensated the expected decrease in CH_4 emissions due to the shrinking of flooded areas caused by the dryness.

Consistent with previous studies, the present findings indicate the important role of ENSO in modulating the variability of CH_4 emissions over the Amazon. Nevertheless, the process described here differs from that documented for regions in the western Pacific. During an El Niño (La Niña) year, the low-level southeasterlies (northwesterlies) in the Indian Ocean region reduce (increase) the horizontal transport of CH_4 from this oceanic region into the western Pacific, where the weakened (intensified) convection due to ENSO contributes to a decrease (increase) in CH_4 in the upper middle troposphere through variations in the vertical transport from the lower levels (Terao et al., 2011). In that study, the authors analyzed the CH_4 variations in the western Pacific, a region outside the source of CH_4 (Indian Ocean), whereas here we analyze the CH_4 variations in its source region (the Amazon basin). Another crucial difference between the ENSO-related CH_4 variations in the western Pacific and those of the Amazon concerns the seasonal cycles of the CH_4 and precipitation. The maximum CH_4 occurs in September, the end of the dry season, in the Amazon. Furthermore, the strongest positive correlations between the southern Oscillation index and the rainfall occur over the northern and northwestern Amazon during austral winter, and over the northern Amazon during austral spring (Rao and Hada, 1990). For all these reasons, we interpret that the ENSO-related local rainfall variations lead to CH_4 variations. ENSO may exert different impacts within the Amazon region. The differences in the CH_4 concentration between the phases of ENSO over the northern Amazon seem to be mostly associated with changes in flooded areas in response to precipitation changes. On the other hand, the intensification (reduction) in biomass burning over the southeastern Amazon during very dry (wet) years explains the increase (decrease) in CH_4 emissions in this region.

We are conscious that version 6 of the AIRS-CH_4 product is now available. Xiong et al. (2015) presented a validation of these data using 1000 aircraft profiles obtained from several campaigns in different years, mainly over areas in North America, the Pacific and the North Atlantic. For the layers 343–441 hPa and 441–575 hPa, they found biases of −0.76% and −0.05%, and RMSEs of 1.56% and 1.16%, respectively. Compared with the validation of version 5 of the AIRS-CH_4 product, with its RMSEs varying from 0.5% to 1.6% (Xiong et al., 2008, 2010), the RMSEs of version 6 have almost the same magnitudes. So, both versions of AIRS-CH_4 contain similar levels of uncertainty, which might not be relevant for the purpose of the present analysis, particularly with respect to the analysis of interannual variation, because we consider de-seasonalized CH_4 over the Amazon region. Nevertheless, given that one of the improvements in the version 6 data is a larger number of retrieval layers, we intend to analyze the CH_4 variability using this new version in a future study. Likely, the results could be better when using the latest version of the AIRS CH_4 product, because of its better quality and greater sensitivity to lower layers in its outputs (Xiong et al., 2015). The results in the present analysis concerning the two main areas over the Amazon, its northern and southeastern sectors, with remarkable interannual variations of CH_4, might be useful for future monitoring of the variation

in the concentration CH_4, the second-most important greenhouse gas, in this area.

Acknowledgements. This work was part of the MSc Dissertation of the first author, produced under the Post-Graduate Program in Climate and Environment, (CLIAMB, INPA/UEA), with financial support from the Coordination for the Improvement of Higher Education Personnel of Brazil (CAPES). The authors thank the Funding Authority for Studies and Projects of Brazil (FINEP/REMCLAM-UEA) and Amazonas State Research Foundation (FAPEAM) (PROESTADO and GOAMAZON) for research support. The first and third authors were partially supported by the National Council for Technology Science and Development (CNPq) of Brazil. The fourth author thanks FAPEAM for the Senior Visiting Researcher fellowship. The authors thank the two anonymous reviewers for their useful comments and suggestions.

REFERENCES

Basso, L. S., 2014: Determination of the methane emissions in the Amazon Basin (in Portuguese). PhD dissertation, University of São Paulo, Instituto de Pesquisas Energéticas e Nucleares-Centro de Química e Meio Ambiente, São Paulo, 103 pp.

Bousquet, P., and Coauthors, 2006: Contribution of anthropogenic and natural sources to atmospheric methane variability. *Nature*, **443**, 439–443, doi: 10.1038/nature05132.

Bousquet, P., and Coauthors, 2011: Source attribution of the changes in atmospheric methane for 2006-2008. *Atmos. Chem. Phys.*, **11**, 3689–3700, doi: 10.5194/acp-11-3689-2011.

Chen, Y. H., and R. G. Prinn, 2006: Estimation of atmospheric methane emissions between 1996 and 2001 using a three-dimensional global chemical transport model. *J. Geophys. Res*., **111**, D10307, doi: 10.1029/2005JD006058.

Ciais, P., and Coauthors, 2013: Carbon and other biogeochemical cycles. *Climate Change 2013: The Physical Science Basis. Contribution of Working Group I to the Fifth Assessment Report of the Intergovernmental Panel on Climate Change*, T. F. Stocker et al., Eds., Cambridge University Press, Cambridge, United Kingdom and New York, NY, USA. [Available online at http://www.climatechange2013.org/.].

Costa, P. S., R. A. F. Souza, R. V. A. Souza, and E. F. Cartaxo, 2011: Variability of the tropospheric methane concentration over the Hydro-electric Balbina reservoir from the information of the EOS/Aqua satellite. *XV Simpósio Brasileiro de Sensoriamento Remoto*, No. 15, Curitiba-PR. (In Portuguese)

Cressot, C., and Coauthors, 2014: On the consistency between global and regional methane emissions inferred from SCIAMACHY, TANSO-FTS, IASI and surface measurements. *Atmos. Chem. Phys.*, **14**, 577–592, doi: 10.5194/acp-14-577-2014.

Dlugokencky, E. J., K. A. Masarie, P. M. Lang, and P. P. Tans, 1998: Continuing decline in the growth rate of the atmospheric methane burden. *Nature*, **393**, 447–450, doi: 10.1038/30934.

Dlugokencky, E. J., and Coauthors, 2009: Observational constraints on recent increases in the atmospheric CH_4 burden. *Geophys. Res. Lett*., **36**, L18803, doi: 10.1029/2009GL039780.

Fisch, G., J. A. Marengo, and C. A. Nobre, 1998: Uma revisão geral sobre o clima da Amazônia. *Acta Amazonica*, **28**, 101–126.

Hodson, E. L., B. Poulter, N. E. Zimmermann, C. Prigent, and J. O. Kaplan, 2011: The El Niño-Southern Oscillation and wetland methane interannual variability. *Geophys. Res. Lett*., **38**, L08810, doi: 10.1029/2011GL046861.

Huffman, G. J., and Coauthors, 2007: The TRMM multisatellite precipitation analysis (TMPA): Quasi-global, multiyear, combined-sensor precipitation estimates at fine scales. *Journal of Hydrometeorology*, **8**, 38–55.

IPCC, 2013: Summary for policymakers. *Climate Change 2013: The Physical Science Basis. Contribution of Working Group I to the Fifth Assessment Report of the Intergovernmental Panel on Climate Change*, T. F. Stocker et al., Eds., Cambridge University Press, Cambridge, United Kingdom and New York, NY, USA. [Available online at http://www.climatechange 2013.org/].

Junk, W. J., 1970: Investigations on the ecology and production biology of the "floating Meadows" (*Paspalo-Echinochloetum*) on the middle Amazon, Part I: The floating vegetation and its ecology. *Amazoniana*, **2**, 449–495.

Kirschke, S., and Coauthors, 2013: Three decades of global methane sources and sinks. *Nature Geosci.*, **6**, 813–823, doi: 10.1038/ngeo1955.

Le Marshall, J., and Coauthors, 2006: Improving global analysis and forecasting with AIRS. *Bull. Am. Meteor. Soc*., **87**, 891–894.

Levin, I., and Coauthors, 2012: No inter-hemispheric δ^{13} CH_4 trend observed. *Nature*, **486**, E3-E4, doi: 10.1038/nature 11175.

Lewis, S. L., P. M. Brando, O. L. Phillips, G. M. F. van der Heijden, and D. Nepstad, 2011: The 2010 Amazon drought. *Science*, **331**, 554, doi: 10.1126/science.1200807.

Melack, J. M., and L. L. Hess, 2011: Remote sensing of the distribution and extent of wetlands in the Amazon Basin. *Amazonian Floodplain Forests: Ecophysiology, Biodiversity and Sustainable Management*, W. J. Junk et al., Eds., Springer, Netherlands, 43–59, DOI: 10.1007/978-90-481-8725-6-3.

MCTI. 2013: Annual estimates of the greenhouse emissions over Brazil. Ministério da Ciência, Tecnologia e Inovação, Brasília-DF, 80 pp. (In Portuguese)

Park, M., W. J. Randel, D. E. Kinnison, R. R. Garcia, and W. Choi, 2004: Seasonal variation of methane, water vapor, and nitrogen oxides near the tropopause: Satellite observations and model simulations. *J. Geophys. Res*., **109**, D03302, doi: 10.1029/2003JD003706.

Pison, I., B. Ringeval, P. Bousquet, C. Prigent, and F. Papa, 2013: Stable atmospheric methane in the 2000s: key-role of emissions from natural wetlands. *Atmos. Chem. Phys.*, **13**, 11 609–11 623, doi: 10.5194/acpd-13-9017-2013.

Rajab, J. M., M. Z. MatJafri, and H. S. Lim, 2012: Methane interannual distribution over peninsular Malaysia from atmospheric infrared sounder data: 2003–2009. *Aerosol and Air Quality Research*, **12**, 1459–1466, doi: 10.4209/aaqr.2012.02.0039.

Rao, V. B., and K. Hada, 1990: Characteristics of rainfall over Brazil: Annual and variations and connections with the Southern Oscillation. *Theor. Appl. Climatol*., **42**, 81–91.

Richey, J. E., R. H. Meade, E. Salati, A. H. Devol, C. F. Nordin Jr., and U. D. Santos, 1986: Water discharge and suspended sediment concentrations in the Amazon River: 1982-1984. *Water Resour. Res*., **22**, 756–764.

Ringeval, B., N. de Noblet-Ducoudré, P. Ciais, P. Bousquet, C. Prigent, F. Papa, and W. B. Rossow, 2010: An attempt to quantify the impact of changes in wetland extent on methane emissions on the seasonal and interannual time scales. *Global Biogeochemical Cycles*, **24**, GB2003, doi: 10.1029/2008GB003354.

Sawakuchi, H. O, D. Bastviken, A. O. Sawakuchi, A. V. Krusche, M. V. R. Ballester, and J. E. Richey, 2014: Methane emissions from Amazonian Rivers and their contribution to the global methane budget. *Global Change Biology*, **20**, 2829–2840.

Simpson, I. J., F. S. Rowland, S. Meinardi, and D. R. Blake, 2006: Influence of biomass burning during recent fluctuations in the slow growth of global tropospheric methane. *Geophys. Res. Lett*., **33**, L22808, doi: 10.1029/2006GL027330.

Simpson, I. J., M. P. S. Andersen, S. Meinardi, L. Bruhwiler, N. J. Blake, D. Helmig, F. S. Rowland, and D. R. Blake, 2012: Long-term decline of global atmospheric ethane concentrations and implications for methane. *Nature*, **488**, 490–494, doi: 10.1038/nature11342.

Susskind, J., C. D. Barnet, and J. M. Blaisdell, 2003: Retrieval of atmospheric and surface parameters from AIRS/AMSU/HSB data in the presence of clouds. *IEEE Trans. Geosci. Remote Sens*., **41**, 390–409.

Tate, K. R., 2015: Soil methane oxidation and land-use change—from process to mitigation. *Soil Biology and Biochemistry*, **80**, 260–272, doi: 10.1016/j.soilbio.2014.10.010.

Terao, Y., H. Mukai, Y. Nojiri, T. Machida, Y. Tohjima, T. Saeki, and S. Maksyutov, 2011: Interannual variability and trends in atmospheric methane over the western Pacific from 1994 to 2010. *J. Geophys. Res*., **116**, D14303, doi: 10.1029/2010JD015467.

Torrence, C., and G. P. Compo, 1998: A practical guide to wavelet analysis. *Bull. Amer. Meteor. Soc*., **79**, 61–78.

Torrence, C., and P. J. Webster, 1999: Interdecadal changes in the ENSO-monsoon system. *J. Climate*, **12**, 2679–2690.

UNFCCC, 2008: Kyoto Protocol Reference Manual: On accounting of emissions and assigned amount. United Nations Framework Convention on Climate Change, 122 pp. [Available online at: http://unfccc.int/resource/docs/publications/08_unfccc_kp_ref_manual.pdf].

van der Werf, G. R., J. T. Randerson, L. Giglio, G. J. Collatz, P. S. Kasibhatla, and A. F. Arellano, 2006: Interannual variability in global biomass burning emissions from 1997 to 2004. *Atmos. Chem. Phys.*, **6**, 3423–3441, doi: 10.5194/acp-6-3423-2006.

Walter, B. P., M. Heimann, and E. Matthews, 2001a: Modeling modern methane emissions from natural wetlands: 1. Model description and results. *J. Geophys. Res*., **106**, 34 189–34 206, doi: 10.1029/2001JD900165.

Walter, B. P., M. Heimann, and E. Matthews, 2001b: Modeling modern methane emissions from natural wetlands: 2. Interannual variations 1982–1993. *J. Geophys. Res*., **106**, 34 207–34 219.

Wilks, D. S., 2006: *Statistical Methods in the Atmospheric Sciences*. 2nd ed., Elsevier , New York, 611 pp.

WMO, 2013: Greenhouse gas bulletin: The state of Greenhouse gases in the atmosphere using global observations through 2012 World Meteorological Organization. [Available online at https://www.wmo.int/pages/prog/arep/gaw/ghg/documents/GHG_Bulletin_No.9_en.pdf].

Worden, J., and Coauthors, 2013: El Niño, the 2006 Indonesian peat fires, and the distribution of atmospheric methane. *Geophys. Res. Lett*., **40**: 4938–4943, doi: 10.1002/grl.50937.

Xiong, X., C. Barnet, J. Wei, and E., Maddy, 2009a: Information-based mid-upper tropospheric methane derived from Atmospheric Infrared Sounder (AIRS) and its validation. *Atmos. Chem. Phys. Discuss.*, **9**, 16 331–16 360.

Xiong, X., S. Houweling, J. Wei, E. Maddy, F. Sun, and C. Barnet, 2009b: Methane plume over South Asia during the monsoon season: satellite observation and model simulation. *Atmos. Chem. Phys.*, **9**, 783–794.

Xiong, X. Z., C. Barnet, E. Maddy, C. Sweeney, X. P. Liu, L. H. Zhou, and M. Goldberg, 2008: Characterization and validation of methane products from the Atmospheric Infrared Sounder (AIRS). *J. Geophys. Res*., **113**, G00A01, doi: 10.1029/2007JG000500.

Xiong, X. Z., C. Barnet, E. Maddy, J. Wei, X. P. Liu, and T. S. Pagano, 2010: Seven years' observation of mid-upper tropospheric methane from atmospheric infrared sounder. *Remote Sensing*, **2**, 2509–2530.

Xiong, X., F. Weng, Q. Liu, and E. Olsen, 2015: Space-borne observation of methane from atmospheric infrared sounder version 6: validation and implications for data analysis. *Atmospheric Measurement Techniques*, **8**, 8563–8597, doi: 10.5194/amtd-8-8563-2015.

Zhang, X. M., X. Y. Zhang, L. J. Zhang, and X. H. Li, 2013: Accuracy comparison of monthly AIRS, GOSAT and SCIAMACHY data in monitoring atmospheric CH4 concentration. *Proc. of the 21st International Conference on Geoinformatics*, IEEE, Kaifeng, 1–4.

Zhang, X. Y., W. G. Bai, P. Zhang, and W. H. Wang, 2011: Spatiotemporal variations in mid-upper tropospheric methane over China from satellite observations. *Chinese Science Bulletin*, **56**, 3321–3327, doi: 10.1007/s11434-011-4666-x.